International Journal of Electrical, Electronic and Communication Sciences
ISSN: 2517-9438
Vol:6, No:5, 2012

New Triangle-Ring UWB Bandpass Filter with Sharp Roll-Off and Dual Notched Bands

Hung-Wei Wu, Yung-Wei Chen, Yu-Fu Chen and Cheng-Yuan Hung

***Abstract*—**This paper presents a new ultra-wideband (UWB) bandpass filter (BPF) with sharp roll-off and dual-notched bands. The filter consists of a triangle ring multi-mode resonator (MMR) with the stub-loaded resonator (SLR) for controlling the two transmission zeros at 2.8 / 11 GHz, the embedded open-circuited stub and the asymmetric tight coupled input/output (I/O) lines for introducing the dual notched bands at 5.2 / 6.8 GHz. The attenuation slope in the lower and higher passband edges of the proposed filter show 160- and 153-dB/GHz, respectively. This study mainly provides a simple method to design a UWB bandpass filter with high passband selectivity and dual-notched bands for satisfying the Federal Communications Commission (FCC-defined) indoor UWB specification

Keywords—steeply slopes transition band, bandpass filter, ultra-wideband (UWB), triangle-ring, multi-mode resonator, stub-loaded resonator.

I. Introduction

ULTRA wideband (UWB) bandpass filters (BPFs) with high performance are desirable in UWB wireless communication systems (from 3.1 to 10.6 GHz) [1]. Recently, the UWB filters with single- or multi-notched bands having the capabilities to avoid the interferences from Wireless Local Area Network systems (WLAN, IEEE 802.11a, 5.15 – 5.825 GHz) and RFID (at 6.8 GHz). Besides, in order to meet UWB radiation limits, steep passband selectivity at lower and higher passband edges in the UWB filter characteristics become more important. Therefore, the design of a compact, high passband selectivity and multi-notched bands UWB bandpass filter is a great challenge to filter designers. UWB bandpass filters with notched bands using multiple-mode resonator (MMR) have been studied [2]–[4]. M. H. Weng *et al*. proposed the UWB filter with single notch band (at 5.8 GHz) [2]. The embedded open-circuited stub is desirable to introduce single narrow-bandwidth notched band for avoiding the interferences from WLAN. Z. C. Hao *et al*. proposed the UWB filter with multiple notch bands by using the multilayer nonuniform periodical structure [3]. The filters with single-, double- and triple-notch bands are implemented on the liquid crystal polymer (LCP) substrate by using thin film fabrication process. K. Song *et al*. proposed the UWB filter with multiple notch bands by using the asymmetric coupling strip [4]. The filter can provide two main paths for the signals, which makes it possible to generate multiple transmission zeros. In order to avoid the interference from the WLAN and RFID signals, the UWB filter with high passband selectivity and multiple notch bands is required. In this paper, we present a new UWB bandpass filter with sharp roll-off and dual-notched bands.

H. W. Wu, Y. W. Chen and Y. F. Chen are with the Department of Computer and Communication, Kun Shan University, 710 Taiwan. (e-mail: hwwu@mail.ksu.edu.tw).

C. Y. Hung is with the Department of Electronics and Computer Science, Tung Fang Design University (e-mail: goliro.goliro@msa.hinet.net)

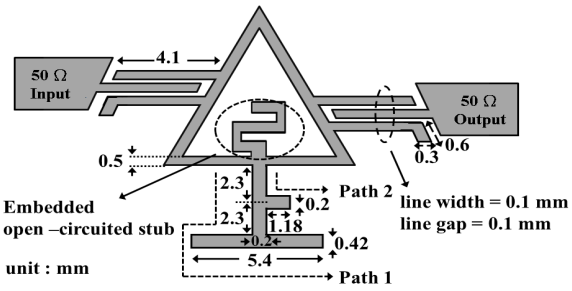

Fig. 1 Configuration of the proposed UWB filter

The filter consists of a triangle ring MMR with stub-loaded resonator for controlling the two transmission zeros at 2.8 / 11, the embedded open-circuited stub and the asymmetric tight coupled input/output (I/O) lines for introducing the dual notched bands at 5.2 / 6.8 GHz. The design theory explains how to control the two transmission zeros and introduce the dual notched bands. The theory and guideline for designing the geometric parameters of the proposed filter are clearly described. The measured results are in good agreement with those obtained from the simulation.

II. Filter Design

The configuration of the filter developed in this paper is shown in Fig. 1. The filter consists of a triangle-ring MMR, stub loaded resonator, embedded open-circuited stub (the total length is equal to λ/4 at 5.2 GHz) and asymmetric tight coupled I/O lines. The substrate used for simulation and fabrication in this study is RT/Duroid 6010 with a dielectric constant (ε_r) of 10.2 and a thickness of 1.27 mm. The proposed filter provides a new structure to have five resonant modes without etching the ground plane. The proposed structure provides enough degrees of freedom for controlling the resonant modes. Fig. 2(a) shows the structure of the proposed resonator. The resonator consists of a triangle-ring multi-mode resonator with characteristic impedance (Z_0) and electrical length ($\theta_1 + \theta_2 + \theta_3 \fallingdotseq 2\pi$), a stub-loaded resonator with two propagation paths (path 1 and path 2) combined with the λ/4-length open-circuited stubs and embedded open-circuited stub with Z_5, θ_8 along the symmetric plane of the filter. The two propagation paths composed of the λ/4-length transmission line sections with (Z_4, θ_7), (Z_1, θ_4) and (Z_3, θ_6) for path 1 and (Z_4, θ_7) and (Z_2, θ_5) for path 2 are designed at around 2.8 ($\theta_4 + \theta_6 + \theta_7 \fallingdotseq \pi/2$) and 11 GHz ($\theta_7 + \theta_5 \fallingdotseq \pi/2$) for generating the lower and upper transmission zeros.

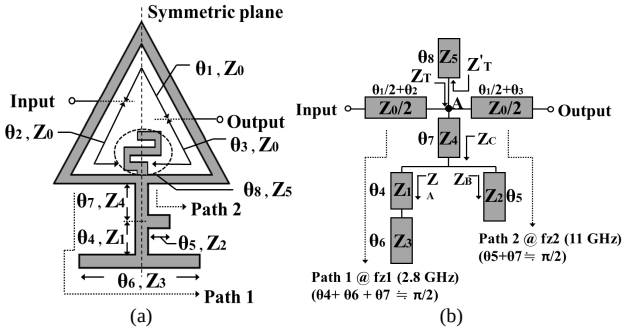

(a) (b)

Fig. 2 (a) Structure and (b) equivalent transmission line model of the proposed triangle-ring multi-mode stub-loaded resonator (MM-SLR). (f_{z1} and f_{z2} : lower / upper transmission zero frequencies and $Z_1 = Z_2 = Z_4$ in this work)

The offset "d" between the I/O ports is the optimum parameter verified by the full-wave EM simulation [5] for obtaining the good UWB passband performance (d = 4.5 mm in this work). Fig. 2(b) shows the equivalent transmission line model of the proposed resonator. Z_A and Z_B are the input impedance looking into either side of the open-circuited stubs. Z_c is the input impedance combined with Z_A and Z_B. Z_T is the total input impedance to Z_c which is looking into the feed point A. Therefore, Z_T can be derived from

$$Z_T = Z_4 \frac{Z_C + jZ_4\tan\theta_7}{Z_4 + jZ_C\tan\theta_7} \quad (1)$$

$$Z'_T = -jZ_5\cot\theta_8 \quad (2)$$

where

$$Z_C = \frac{Z_A Z_B}{Z_A + Z_B} \quad (3)$$

$$Z_A = -j\,Z_1 \frac{Z_3\cot\theta_6 - Z_1\tan\theta_4}{Z_1 + Z_3\cot\theta_6\tan\theta_4} \quad (4)$$

$$Z_B = -j\,Z_2\cot\theta_5 \quad (5)$$

$$Z_3 = -j\,Z_3\cot\theta_6 \quad (6)$$

The ABCD matrix of the stub-loaded resonator can be obtained by

$$[ABCD]_T = [ABCD]_{Input} \times [ABCD]_{MM\text{-}SLR} \times [ABCD]_{Output} \quad (7)$$

where Z_0 = 50 Ω and $\theta_1 \fallingdotseq \pi/2$ at the center frequency of 6.8 GHz. The transmission zeros occurs when S_{21} = 0. The S_{21} parameters are given by [6]

$$S_{21} = \frac{-2Y_{21}Y_0}{(Y_0 + Y_{11})(Y_0 + Y_{22}) - Y_{12}Y_{21}} = 0 \quad (8)$$

$$[ABCD]_T \Rightarrow Y_T,$$

$$Y_{21} = \frac{Z_T}{Z_T(\cos\theta_1/2+\theta_2)(jZ_0/2\sin\theta_1/2+\theta_3)+(jZ_0/2\sin\theta_1/2+\theta_2)(jZ_0/2\sin\theta_1/2+\theta_3)+Z_T(jZ_0/2\sin\theta_1/2+\theta_2)(\cos\theta_1/2+\theta_3)} \quad (9)$$

where Y_0 is the characteristic admittance. It is found that Y_{21} = 0 which gives the conditions of the transmission zeros [7]. By letting Z_T = 0, the stub-loaded resonator behaves can be considered as a short circuit. The transmission zeros can be well determined. In this work, we choose θ_4 = 19° and $\theta_6 + \theta_7$ = 63° (θ_7 = 19°) for 2.8 GHz (f_{Z1}) and θ_5 = 38° and θ_7 = 70° for 11 GHz (f_{Z2}) and Z_3 = 74 Ω and $Z_1 = Z_2 = Z_4$ = 91 Ω for achieving rejection level of transmission zeros better than 30 dB.

Fig. 3 shows the relations between the image admittance [Y_{21}] and locations of the lower transmission zero frequencies (f_{z1}) depending on the electrical lengths (θ_4) and the impedance ratio ($K = Z_1 / Z_3$) of the proposed resonator. The location of lower transmission zero (f_{z1}) can be controlled by electrical length θ_4 and impedance ratio ($K = Z_1 / Z_3$, where Z_3 and Z_4 are fixed) of the path 1, as shown in Fig. 2(b).

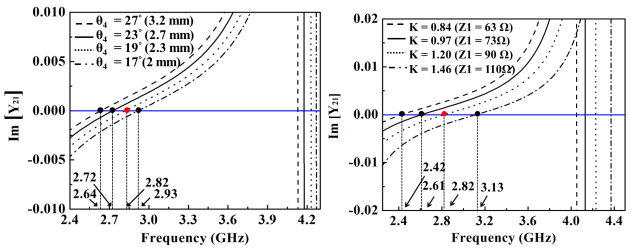

(a) (b)

Fig. 3 Relations between the image admittance [Y_{21}] and locations of the lower transmission zero frequencies (f_{z1}) depending on (a) electrical lengths (θ_4) and (b) impedance ratio ($K = Z_1 / Z_3$) of the proposed resonator. (where θ_6 = 44°, Z_3 = 75 Ω, Z_4 = 91 Ω and θ_7 = 19° are fixed for all cases)

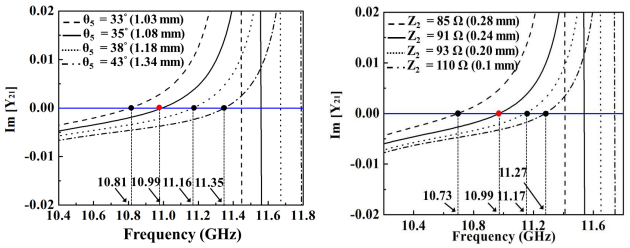

(a) (b)

Fig. 4 Relations between the image admittance [Y_{21}] and locations of the higher transmission zero frequencies (f_{z2}) depending on (a) electrical lengths (θ_5) and (b) impedance section Z_2 of the proposed resonator. (where θ_7 = 19° and Z_4 = 91 Ω are fixed for all cases)

Changing the θ_4 from 43° to 53° (2 to 3.2 mm), f_{z1} is shifted from 2.93 to 2.64 GHz with maintaining of the f_{z2}. Similarly, changing the K from 0.84 to 1.46 (Z_1 = 63 Ω to 110 Ω), f_{z1} is shifted from 2.42 to 3.13 GHz. Fig. 4 shows the relations between the image admittance [Y_{21}]and locations of the higher transmission zero frequencies (f_{z2}) depending on the electrical lengths (θ_5) and the impedance section Z_2 of the proposed resonator. The location of higher transmission zero (f_{z2}) can be controlled by electrical length θ_5 and impedance section Z_2 of the path 2, as shown in Fig. 2(b). Changing the θ_5 from 33° to 43° (1.03 to 1.34 mm), f_{z2} is shifted from 10.81 to 11.35 GHz with maintaining of the f_{z1}. Similarly, changing the impedance section Z_2 from 85 to 110 Ω (0.28 to 0.1 mm), f_{z2} is shifted from 10.73 to 11.27 GHz. It is noted that the S_{21}-magnitude peaks with changing the parameters of path 2 are not enough smooth might due to discontinuity effects of the microstrip line. Fig. 5(a) and (b) show the simulated S_{21}-magnitude with tuning the length of θ_8 and the impedance of Z_5 for embedded open-circuited stub. It is found that the notched band can be controlled by the dimensions of the embedded open-circuited stub, where the length of l_8 dominated the notched band frequencies and the width of W_5 dominated the notched bandwidths.

Similarly, Fig. 5(c) and (d) show the simulated S_{21}-magnitude with tuning the length of θ_9 and the impedance of Z_6 for the asymmetric tight I/O lines. It is clearly observed that with increasing l_8 (correspond to near quarter wavelength at 5.2 GHz) and l_9, the notch bands are shifted to lower frequency and with increasing W_5 and W_6, the bandwidth of the dual notch bands slightly increases.

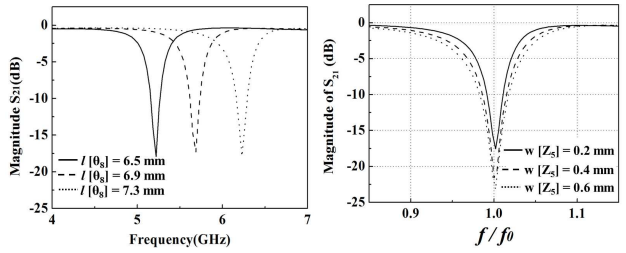

(a) (b)

Fig. 5 Simulated S_{21}-magnitude with tuning (a) the length of θ_8 and (b) the impedance of Z_5 for embedded open-circuited stub

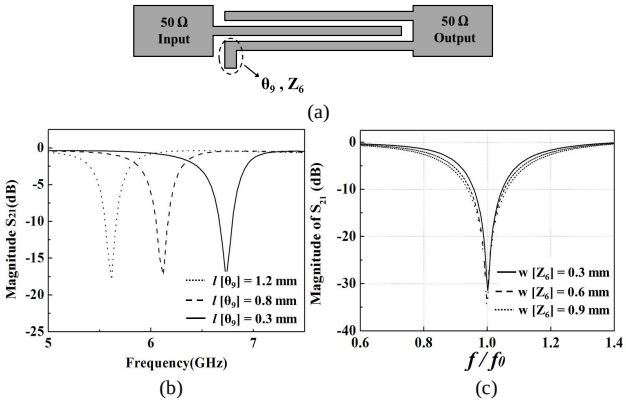

(a) (b) (c)

Fig. 5 (a) Proposed asymmetric tight coupled I/O lines and simulated S_{21}-magnitude with tuning (b) the length of θ_8 and (c) the impedance of Z_5 for embedded open-circuited stub and (c) the length of θ_9 and (d) the impedance of Z_6 for the asymmetric tight I/O lines

III. Results

The size of the fabricated filter is 15 × 8 mm^2, approximately 0.34 λ_0 × 0.18 λ_0, where λ_0 is the guided wavelength of the center frequency (6.8 GHz). Measured results of the filter are characterized in an HP 8510C network analyzer. Fig. 6(a) and (b) show the photograph, measured results and group delay of the fabricated UWB filter. The measured results of the filter have 3-dB fractional bandwidth (FBW) of 110%, average return loss (-20 log $|S_{11}|$) of around 20 dB, average insertion loss (-20 log $|S_{21}|$) of around 0.6 dB and two transmission zeros located at 2.8 / 11 GHz. The dual notched bands are located on 5.2 and 6.8 GHz. The measured group delay is also shown in Fig. 6(b). The attenuation slope in the lower and higher passband edges is 160- and 153-dB/GHz, respectively. Table I summarized the comparison of the proposed filter with other reported UWB filters [3], [4] and [8]. The mismatch between the simulated and measured results might be due to the fabrication errors or the variation of material properties.

The superior features indicate that the BPF has a potential to be utilized in the modern ultra-wideband wireless communication systems.

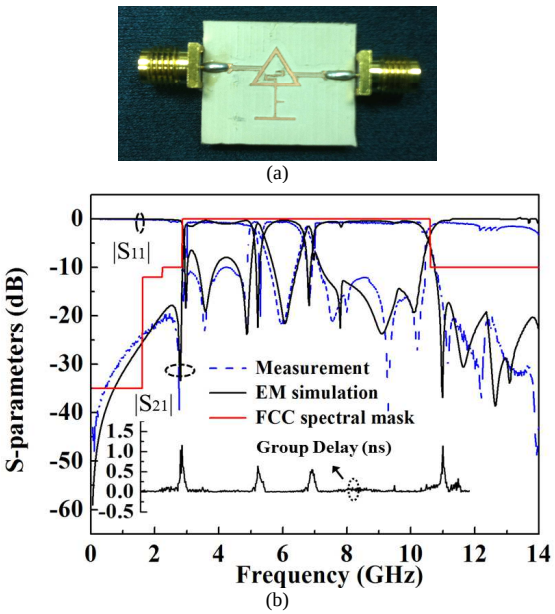

(a) (b)

Fig. 6 (a) Photograph, (b) measured results and group delay of the fabricated UWB filter

TABLE I
COMPARISONS WITH OTHER PROPOSED UWB FILTERS. (PCB: PRINTED CIRCUIT BOARD; FBW: 3-DB FRACTIONAL BANDWIDTH; Λ_0 IS THE FREE-SPACE WAVELENGTH OF THE CENTER PASSBAND FREQUENCY)

	Ref. [3]	Ref. [4]	Ref. [8]	**Proposed filter**
Substrate height (mm) / ε_r	(LCP) 0.8 / 3.15	(PCB) 0.787 / 2.2	(PCB) 1 / 2.2	**(PCB) 1.27 / 10.2**
Return loss (dB)	25	15	20	**20 (max.)**
Insertion loss (dB)	< 0.66	< 0.8	< 0.5	**< 0.5 (min.)**
Notch band 1				
Center freq. (GHz) / Rejection level (dB)/ FBW (%)	5.47 / 25.38 / 3.1	4.3 / ~20 / 4.2	5.8 / ~15 / 7.9	**5.2 / 22 / 4**
Notch band 2				
Center freq. (GHz) / Rejection level (dB)/ FBW (%)	6.05 / 29.9 / 3.6	8 / ~20 / 3.8	8 / ~15 / 6.4	**6.8 / 18 / 5**
3-dB FBW (%)	109	110	118	**110**
Circuit Size (mm^2) ($\lambda_0 \times \lambda_0$)	406 (0.5×0.4)	63.72 (0.53×0.06)	680 (0.78×0.46)	**120 (0.34×0.18)**

IV. Conclusion

A new UWB filter with high passband selectivity using stub-loaded resonators is presented. The proposed multi-mode stub-7 loaded resonator provides two transmission zeros which are designed at 2.8 and 11 GHz to provide the good passband selectivity with 160- and 153-dB/GHz slopes. It is also verified that the asymmetric tight coupled I/O lines are necessary for introducing the UWB frequency response by using the image-parameter method and the EM simulation. Both measured and simulated results are in good agreement.

The proposed BPF is very useful for the modern UWB wireless communication system.

ACKNOWLEDGMENT

The authors would like to acknowledge funding support from the Nation Science Council of Taiwan under Grant NSC 100-2221-E-272-003 and NSC 100-2628-E-168-001-MY2.

REFERENCES

[1] O. "Revision of Part 15 of the Commission's Rules Regarding Ultra-Wideband Transmission Systems," First Note and Order Federal Communications Commission, ET-Docket 98–153, 2002.
[2] M. H. Weng, C. T. Liauh, H. W. Wu and S. R. Vargas, "An ultra-wideband bandpass filter with an embedded open-circuited stub structure to improve in-band performance," IEEE Microw. Wireless Compon. Lett, vol. 19, no. 3, pp. 146–148, 2009.
[3] Z. C. Hao, J. S. Hong , "Ultra-wideband bandpass filter with multiple notch bands using nonuniform periodical slotted ground structure", IEEE Trans. MTT., pp. 3080–3088, 2009.
[4] K. Song, and Q. Xue, "Compact ultra-wideband (UWB) bandpass filter with Multiple notch bands," IEEE Microw. Wireless Compon. Lett., pp. 447-449, 2010.
[5] IE3D Simulator, Zeland Software, Inc., 2002.
[6] K. Ma, K. S. Yeo, J. Ma and M. A. Do, "An ultra-compact hairpin band pass filter with additional zero point," IEEE Microw. Wireless Compon. Lett, vol. 17, no. 4, pp. 262–264, 2007.
[7] K. S. Chin, Y. C. Chiang and J. T. Kuo"Microstrip open-loop resonator with multispurious suppression," IEEE Microw. Wireless Compon. Lett, vol. 17, no. 8, pp. 574–576, 2007.
[8] F. Wei, Q. Y. Wu, X. W. Shi and L. Chen, "Compact UWB bandpass filter with dual notch bands based on SCRLH resonator, " IEEE Microw. Wireless Compon. Lett., pp.28–30, 2010.